Title
INELASTIC SCATTERING OF 12-Mev PROTONS ON LITHIUM, CARBON, MAGNESIUM, AND SILICON

Author
Conzett, Homer E.

Publication Date
1956-04-06

UCRL 3371

UNIVERSITY OF CALIFORNIA

Radiation Laboratory

BERKELEY, CALIFORNIA

DISCLAIMER

UCRL-3371

UNIVERSITY OF CALIFORNIA

Radiation Laboratory
Berkeley, California

Contract No. W-7405-eng-48

INELASTIC SCATTERING OF 12-Mev PROTONS ON LITHIUM, CARBON, MAGNESIUM, AND SILICON

Homer E. Conzett

(Thesis)

April 6, 1956

Printed for the U. S. Atomic Energy Commission

INELASTIC SCATTERING OF 12-Mev PROTONS ON LITHIUM, CARBON, MAGNESIUM, AND SILICON

Contents

INELASTIC SCATTERING OF 12-Mev PROTONS ON LITHIUM, CARBON, MAGNESIUM, AND SILICON

Homer E. Conzett

Radiation Laboratory
University of California
Berkeley, California

April 6, 1956

ABSTRACT

The angular distributions of protons from the reactions

$Li^7(p, p')Li^{7*}$, Q = -4.61 Mev;
$C^{12}(p, p')C^{12*}$, Q = -4.43 Mev;
$Mg^{24}(p, p')Mg^{24*}$, Q = -1.36 Mev; and
$Si^{28}(p, p')Si^{28*}$, Q = -1.78 Mev

have been measured, and the cross sections for the reactions have been obtained.

The lithium distribution has been analyzed in terms of, (a) inelastic scattering proceeding through formation and decay of the compound nucleus, and (b) direct inelastic scattering of the Austern, Butler, McManus theory, the selection rules of which permit the assignment of J = 1/2, 3/2, or 5/2 and odd parity to the 4.61-Mev level of Li^7. The carbon, magnesium, and silicon distributions indicate that the statististical theory of the compound nucleus does not apply and, also, that the direct interaction type of scattering is negligible. It appears that the reactions involving these nuclei proceed through only a few or several levels of the intermediate nuclei.

For each reaction, the cross section has been compared with estimates of the cross section for formation of the compound nucleus. The results are in qualitative agreement with the theory of decay of the compound nucleus through competing channels.

I. INTRODUCTION

The inelastic scattering of protons was first observed in 1940,[1] resulting from the bombardment of aluminum and neon with 6.9- and 4-Mev protons respectively. Since then, the technique of inelastic scattering has been employed extensively and has been a valuable method for the determination of nuclear energy levels. The scattering nucleus is excited at the expense of the kinetic energy of the incoming proton; the maximum possible excitation is the available energy in the center-of-mass system. Thus the excitation energy of the residual nucleus is equal to the proton energy loss, measured in the center-of-mass coordinate system. Angular distributions of these inelastically scattered particles can be expected to give more detailed information concerning the nature of the process because these distributions must reflect the additional requirements of conservation of angular momentum and parity.

At present, two theories exist that attempt to explain and predict angular distributions of nuclear reaction products, including inelastically scattered particles. The first is based on the Bohr assumption[2] of the formation and subsequent decay of a compound nucleus, applicable for bombarding energies below 50 Mev. The incident proton and target nucleus form an intermediate (compound) system whose lifetime is sufficient to allow the energy brought in by the incident particle to be shared among all the nucleons. Among the competing modes of decay of this system, that of proton emission, leaving the residual nucleus in an excited state, is the mechanism of inelastic scattering. On the basis of this Bohr assumption, a detailed partial-wave analysis of nuclear reactions[3] yields the theoretical angular distributions. If the reaction proceeds through a single level of the compound nucleus, the distribution is symmetric about the center-of-mass scattering angle $\theta = 90^{\circ}$. If more than one level is important in the reaction, the distribution can become more complex because interference terms between outgoing waves of different parity are present in the expression for the differential cross sections. Finally, if the reaction proceeds through the continuum region of the

compound nucleus, the region of excitation where the level width exceeds the level spacing, and many levels are involved, the theory[4] takes a statistical average over them and assumes that the interference terms between outgoing waves of different parity cancel out; this again results in an angular distribution that is symmetric about $\theta = 90^{\circ}$.

The second theory, proposed by Austern, Butler, and McManus,[5] can be applied to (n, p), (p, n), (n, n'), and (p, p') reactions in the 10-to-30-Mev energy range. They consider the mechanism to be a direct interaction between the incident proton (for inelastic proton scattering) and a nucleon in the surface region of the target nucleus, the interaction taking place outside of the nuclear potential well. That is, if the concept of the nuclear shell model[6] is applied, the bound nucleon participating in the collision is considered to be in a state of definite orbital angular momentum, this state being described by a single-particle wave function with an exponentially decreasing tail outside the potential well. During the time this nucleon spends outside the nucleus, the direct proton-nucleon scattering can occur, uninfluenced by the presence of the rest of the nucleus. This treatment results in angular distributions of inelastically scattered protons of the form

$$\frac{d\sigma}{d\Omega} \propto \sum_{\ell} [C_{\ell} j_{\ell}(qa)]^2 ,$$

where ℓ represents the change of orbital angular momentum (in units of $\hbar$) between the ground state and excited state of the target nucleus and is restricted to the values $\ell_i + \ell_f \geq \ell \geq |\ell_i - \ell_f|$, where ℓ_i and ℓ_f designate the orbital momentum values of the single-particle ground and excited states. Conservation of parity requires that ℓ take only all odd or even values in this range. For given values of ℓ_i and ℓ_f, C_{ℓ} is a coefficient depending only on ℓ; $j_{\ell}(qa)$ is the regular spherical Bessel function of order ℓ;

$$q = |\vec{k}_i - \vec{k}_f| = [(k_i - k_f)^2 + 4k_i k_f \sin^2 \theta/2]^{1/2}$$

is the magnitude of the vector difference between the wave numbers of the incident and scattered proton; and a is the radius of the target nucleus. Since the total angular momentum carried by the single

nucleon in each of the two states is

$$j_i = \ell_i \pm 1/2 \text{ and } j_f = \ell_f \pm 1/2,$$

the possible magnitudes of the vector

$\ell_i - \ell_f$ are $|\vec{j}_i - \vec{j}_f + \vec{l}|$ where $\vec{l}$ arises from cases involving spin flip. Also,

$\vec{j}_i - \vec{j}_f = \vec{J}_i - \vec{J}_f$, where J_i and J_f are the initial and final spins of the target nucleus, so the possible values of ℓ are given by

$$J_i + J_f + 1 \geq \ell \geq |\vec{J}_i + \vec{J}_f + \vec{l}|_{min},$$

and ℓ can take only odd or even values corresponding to a change or no change of nuclear parity.

Angular distributions of protons scattered inelastically from Mg^{24}, exciting the nucleus to 1.368 Mev, have been measured at proton energies of 4.7, 7.3, 9.6, and 10 Mev.[7-10] They are all asymmetric about $\theta=90^{\circ}$, and Fischer's analysis of his 10-Mev results is based on a combination of distributions given by the statistical theory of the compound nucleus and by the direct interaction theory. Similar experiments[8,11,10,12] have been done on the 4.43-Mev level of C^{12} at 7.3, 9.5, 10, and 31 Mev. The shape of the distribution changes little in going from 7.3 to 10 Mev, but that at 31 Mev is peaked strongly at forward angles, thereby showing the predominance of a direct-interaction type of scattering. Similarly, results on the 822-kev level of Fe^{56} at 17 Mev[13] and on several levels of Be^{9} at 31 Mev[14] are peaked near the forward direction.

The experiments described here were undertaken to extend the measurements on C^{12} and Mg^{24} to the energy region of 12-Mev protons and to investigate in the same manner the inelastic scattering from levles in Li^{7} and Si^{28}. The observed angular distributions are compared with those derived from the existing theories.

II. EXPERIMENTAL METHOD

A. General Procedure

A diagram of the experimental arrangement is shown in Fig. 1. The external 12-Mev proton beam of the Crocker Laboratory 60-inch cyclotron was directed at a thin target located at the center of an evacuated scattering chamber. After passing through the target, the beam was collected in a Faraday cup located behind the chamber. Protons scattered from the target were detected by a telescope of three proportional counters contained within a single vacuumtight unit. A remotely controlled absorber changer, permitting insertion of variable amounts of aluminum absorber, was located between the telescope and an aperture defining the solid angle for scattering. Protons of the particular energy under investigation were required to pass through an appropriate amount of absorber and to stop in the range foil separating the second and third counters. Thus, per unit of charge collected in the Faraday cup, the protons with a range between R and $R + \Delta R$ were counted. A plot of these counts versus range gave the differential range curve of the proton group. Since the area under such a curve is proportional to the number of protons that stopped in the range spanned by the curve, measurement of these areas as a function of scattering angle yielded the relative differential cross sections. Determinations of target thickness, the solid angle for scattering, and the ΔR of the detector provided the information necessary for the calculation of the absolute differential cross sections.

B. Beam Alignment

The deflected cyclotron beam passed through a 1/8-inch collimating probe slit and was centered on the cyclotron target port. A magnetic shielding channel was then positioned to bring the beam through the fringing magnetic field and to center it at the channel exit. The beam then traveled through a 1.5-inch-diameter brass pipe to the scattering chamber, located outside the water shielding. A strong-focusing magnetic quadrupole lens, located at the entrance end of the brass pipe, focused the beam to a 1/4-inch-diameter spot at the target

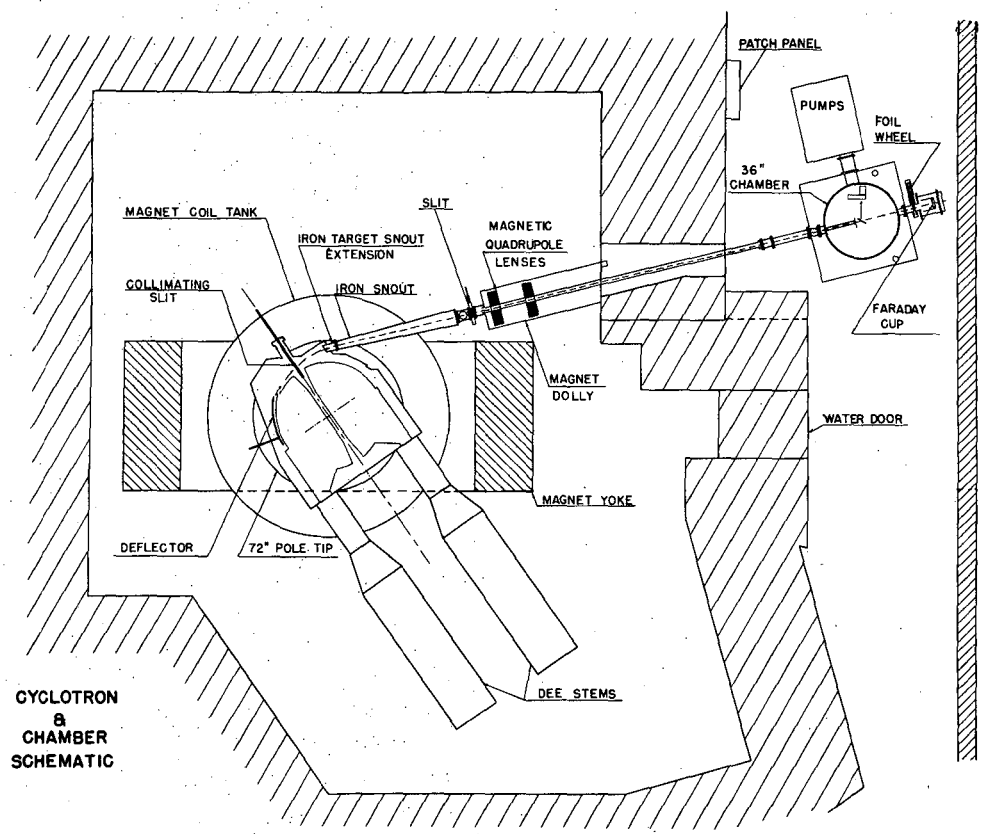

Fig. 1. Diagram of the experimental arrangement.

position in the center of the chamber. A collimating section containing three carbon slits, located inside the chamber, reduced the beam diameter at the target to 1/8 inch.

Nuclear emulsion burn patterns were used to define the beam position, and when the focused beam had been centered at the exit end of the brass pipe, the scattering chamber was adjusted to the beam line. This was done by mounting a telescope on the chamber exit port, aligning it with the collimator section, and then adjusting the chamber until the line of sight was coaxial with the brass pipe. Finally, burn patterns were taken at the exit end of the collimating section with the slits removed. Fine adjustments were made on the chamber position, if necessary, to center the beam in the collimating section, and the slits were replaced. With the collimating slits in position, beam magnitudes of 0.5 microampere through the target could be obtained at normal cyclotron operation.

C. Scattering Chamber

The scattering chamber is 13 inches deep and 36 inches in internal diameter. It contains a remotely controlled rotating table which can be positioned in angle to within 0.1°, its position being transmitted to the control station by means of a selsyn repeater system. The counter and associated equipment were mounted on the table on a radially scribed line which parallels the beam position when the table position is set at 0°. An accurate check on the detector position was made by rotating the table to 180° and sighting on the detector aperture with the previously aligned telescope. The detector dimensions permitted measurements at scattering angles from 7° to 167°.

A remotely controlled target holder is mounted on the lid of the scattering chamber. This provides vertical travel, for the placement of different targets in the beam; rotation about the vertical axis permitted changes in the target angle, accurate to 0.2°.

A local pumping system, consisting of a refrigerated 6-inch diffusion pump backed by a Kinney mechanical pump, maintained pressures near 10^{-4} mm of Hg during operation.

D. Beam Monitoring and Beam-Energy Determination

A Faraday cup mounted on the exit port of the scattering chamber collected the beam. It was isolated from the chamber by an aluminum foil and was evacuated by a separate pumping system. A set of two C-shaped permanent magnets provided a field of about 200 gauss to prevent loss of secondary electrons ejected from the beam-stopping plate under proton bombardment. The collected charge was integrated on a capacitor of known value, and the potential across the capacitor was measured by a dc feedback electrometer whose output was fed into a Speedomax recording voltmeter. The capacitors used were calibrated against one whose value was certified by the Bureau of Standards within 0.1%. The system consisting of the electrometer and recording voltmeter was calibrated against a known input voltage, measured to within 0.2% with a Leeds-Northrup potentiometer.

An auxiliary monitor consisted of a NaI crystal scintillator viewed by a DuMont-6292 photomultiplier tube. Placed outside the scattering chamber, this counter detected particles scattered through an angle of about 18°. Its amplified output pulses, RC clipped to 2 microseconds, were fed into a gate-forming circuit. These gate pulses were monitored with a scaler in the counting area and, in addition, were fed into a counting-rate meter located in the cyclotron control room. This indicator aided the operator in his control of the beam into the scattering chamber.

The energy of the beam was measured by determining its range in aluminum absorber. Two remotely controlled, twelve-position foil wheels were located between the scattering chamber and the Faraday cup. The appropriate foil in one wheel was placed in the beam to reduce its residual range to about 10 mg/cm^2. The other wheel provided foils in steps of 1.53 mg/cm^2. As this wheel rotated, the Faraday cup current was plotted on the recorder chart, giving the integral number-range curve of the beam. The mean range was readily determined to within 0.4%.

An estimate of the energy spread in the beam was obtained from the integral range curve. That is, the width of the differential curve derived from it was measured. Comparison of this spread with the theoretical spread due only to range straggling yielded the spread in beam energy. For example, the largest measured percentage range spread ($100 \times \frac{\text{width}}{\text{mean range}}$) was 3.37%. Unfolding the theoretical range straggling of 2.95% results in a 1.63% range spread in the beam itself. This corresponds to a 0.93% spread in the beam energy at a mean energy of 12 Mev.

E. Detector and Electronics

A schematic diagram of the detector arrangement is shown in Fig. 2. The remotely controlled absorber changer, located between the collimator and the proportional counter telescope, consisted of twelve aluminum absorbers. The thinnest was 0.30 mg/cm^2 and each succeeding one was very nearly twice the value of its predecessor; the thickest one was 615.4 mg/cm^2. Any desired combination of these absorbers could be inserted from the control station in the counting area.

The three proportional counters were contained in a common enclosure filled with a mixture of argon and 4% carbon dioxide to a pressure of one atmosphere. The sensitive volume of each was 0.5 inch deep and approximately 2 inches square. The counters were operated near 1500 volts, with each counter having a separate high voltage supply regulated to 0.1%. A detailed description of this counter telescope and its characteristics has been given by Ellis.[15]

The counter pulses were delay-line clipped to 1 microsecond and then fed into preamplifiers at the scattering chamber. After further amplification by linear amplifiers, the signals were passed through pulse-height discriminators and variable-delay circuits and formed into gates for use in the coincidence circuits. A simplified block diagram of this arrangement is shown in Fig. 3. Double coincidences between the first and second counters and triple coincidences among the three counters were monitored with scalers. The difference between the doubles and triples gave the number of particles that had

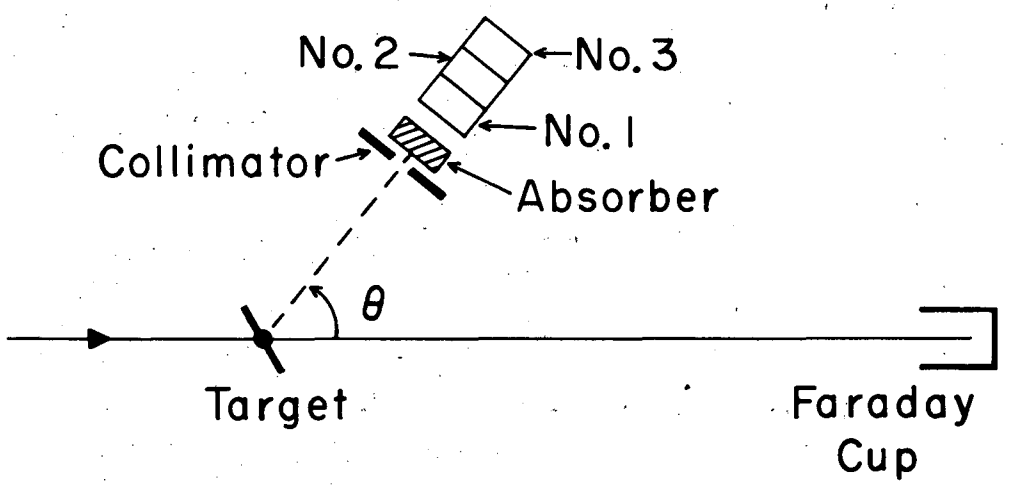

Fig. 2. Schematic diagram of the counter arrangement.

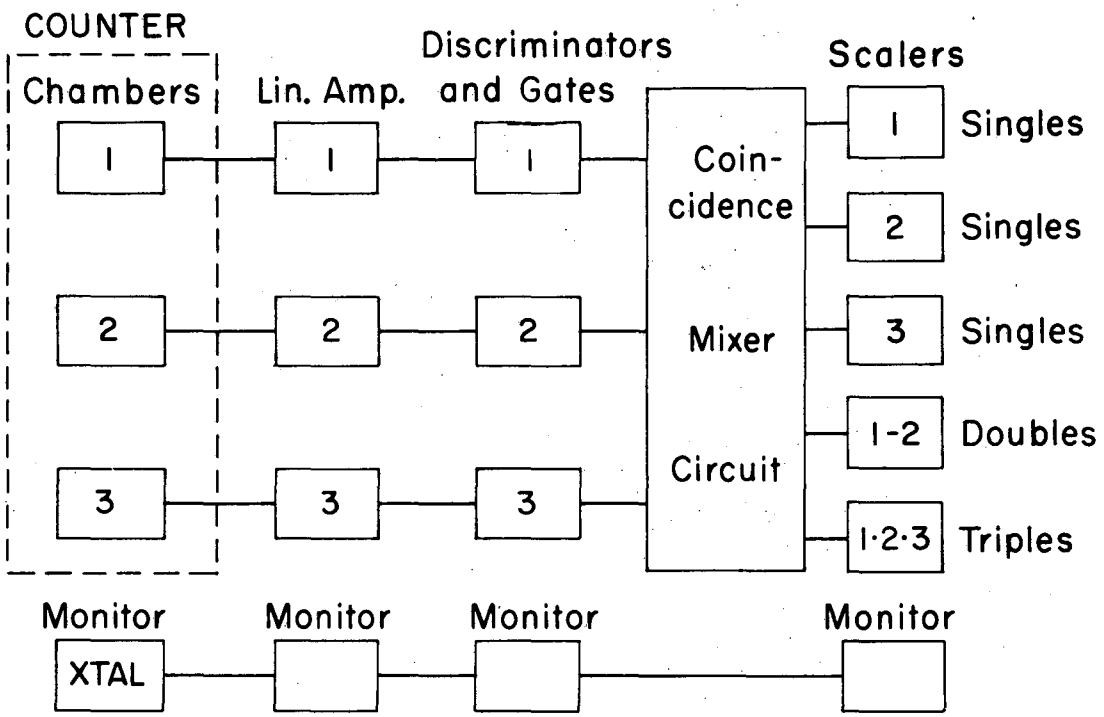

Fig. 3. Block diagram of the electronics.

stopped in the ΔR range foil between the second and third counters. In addition, counts obtained with the first two counters in coincidence and the third in anticoincidence were monitored, but it was found that this circuit was not reliable when the doubles and triples counting rates were simultaneously high. Therefore, the doubles and triples were always recorded and their differences taken.

F. Targets

Special techniques were employed in making and handling the lithium target so that contamination was minimized. In an argon-filled dry box, a freshly cut piece of lithium was sandwiched between two polished steel flats and pressed to the desired thickness of 3 to 4 mils. This was mounted on a target frame, and the assembly was placed in a container which sealed the lithium-bearing section of the frame in an argon atmosphere. The exposed end of the target frame was connected to the target holder in the scattering chamber. After the chamber had been pumped down, the target holder was raised while the container was held in a fixed position, thus separating the two. The target was then adjusted vertically until it was centered on the beam line. Since the target could not be handled for weighing, its thickness (in mg/cm^2) was determined indirectly. The beam's mean range in aluminum was determined with the target in the beam (perpendicular to it) and with the target removed. The difference in range gave the thickness of the target in aluminum equivalent. This was converted to mg/cm^2 of lithium, using the range-energy data of Aron, Hoffman, and Williams.[16] It is believed that this determination of the target thickness was accurate to 5%.

A 2-mil polystyrene $(CH)_n$ foil was used for the carbon target. The proton group corresponding to excitation of the 4.43-Mev level of C^{12} could be resolved from the protons scattered from the hydrogen in the target at all scattering angles except 40°. Thus, this point does not appear in the angular distribution.

The magnesium target was a 0.7-mil foil of normal isotopic material.

Silicon targets were made by employing the vacuum evaporation technique. Silicon monoxide was heated by radiation from tungsten filaments at approximately 2000°C. The evaporated monoxide was deposited on an acetate film, backed by a thin sheet of Electromesh, a fine nickel-plated copper screen mesh, lapped smooth to receive the deposit. The acetate film had been formed by spreading a few drops of a solution of DuPont cement dissolved in amyl acetate on a water surface. After the silicon monoxide was deposited to the desired thickness, a target frame was cemented to the monoxide surface. The backing was then removed by dissolving away the acetate film in a bath of acetone.

G. Measurement of Proton Groups

At a convenient angular position of the detector, sufficient absorber was inserted to place the peak of the elastically scattered proton group in the range bite ΔR of the detector. Counter voltages and linear amplifier gains were adjusted to give pulses of 50 volts mean height from the first and second counters. Discriminator curves were then run on these counters and the discriminator levels set for operation. Figure 4 shows typical discriminator curves with the levels for operation indicated. The curve for counter No. 2 does not show a real plateau because part of the sensitive volume of that counter was included in the detector range bite. That is, a proton was counted as having stopped in the range bite whenever the pulse height from counter No. 2 exceeded the discriminator level, with no corresponding pulse from counter No. 3. As that bias level was lowered, the proton was required to penetrate counter No. 2 less deeply in order to be counted. The effect was that of increasing the detector range bite, and this effect can be seen in the curve of Fig. 4B. The discriminator level for the third counter was set just above the noise level so that triple coincidences were registered for all particles passing through ΔR.

Differential range spectra were obtained by plotting counts (doubles minus triples) against absorber thickness for a unit of charge collected in the Faraday cup. At least one complete range spectrum

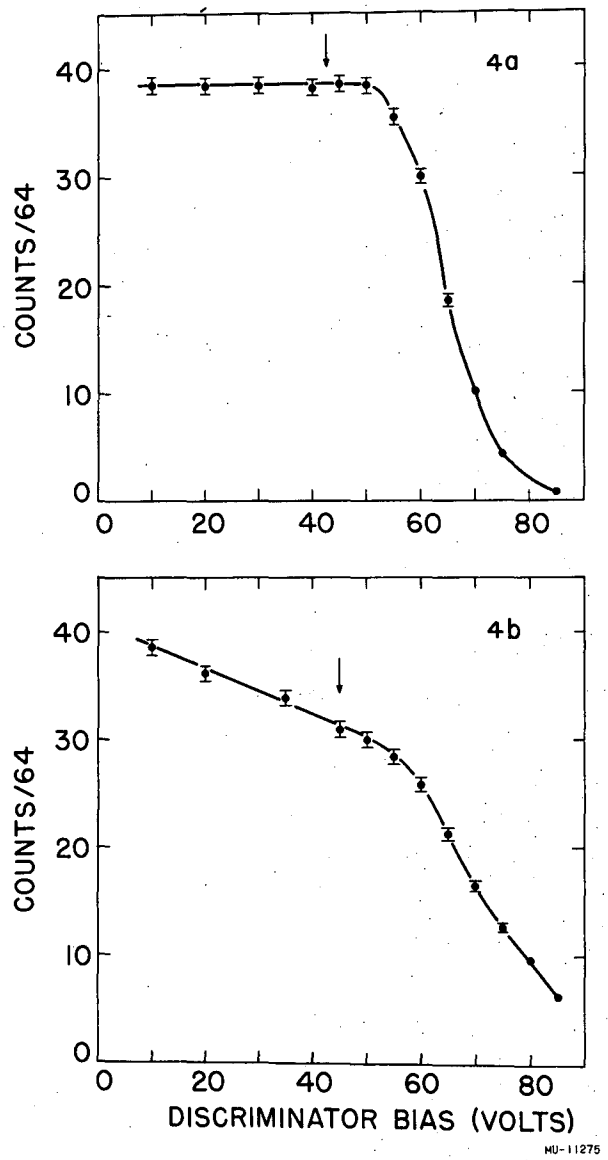

Fig. 4. Typical discriminator curves. A is for counter No. 1 with biases on counters No. 2 and No. 3 fixed. B is for counter No. 2 with biases on counters No. 1 and No. 3 fixed. Arrows indicate bias levels chosen for operation.

was run for each target so that the various particle groups could be noted and identified. Figure 5 shows the spectrum of protons scattered from the polystyrene target at a scattering angle of 50°. The elastic group from carbon was used in the experimental determination of the detector range bite for that run. The quantity measured at each range point R was $(\frac{dN}{dR}\Delta R)$, the product of the number of particles stopping in unit range interval and of the range bite. Thus, the area under the peak is equal to the product of ΔR and the total number of particles stopping in the range interval spanned by the peak,

$$A = \int (\frac{dN}{dR} \Delta R)\, dR = N\Delta R.$$

A determination of N was then made as follows: Absorber corresponding to the value just below the peak was inserted; for example, 160 mg/cm^2 in Fig. 5. The discriminator levels of counters No. 1 and No. 2 were lowered to the point where the pulse heights formed by all the particles in the elastic group exceeded the discriminator levels. Then, the number of doubles coincidences formed per unit of charge collected was just the total number of particles in the group, N. This value, combined with the area under the peak, normalized to the same unit charge collected, gave ΔR. Values of ΔR ranged from 3.09 mg/cm^2 to 3.32 mg/cm^2. These variations from run to run are explained by the fact that the discriminator level for counter No. 2 was not always the same. When this level was set for a particular run, the ΔR remained constant.

Differential range spectra including just the proton group of interest were then taken over the entire range of scattering angles available. In Fig. 5, this was the group corresponding to the excitation of C^{12} to its 4.43-Mev level. Plotting the relative areas under the peaks against scattering angle, gave the angular distribution of the relative differential cross section in the laboratory system.

In order to avoid errors introduced by possible nonuniform target materials, target movement during the runs was minimized. In runs on carbon and silicon the targets were positioned at an angle of 45° to the beam for the entire angular distributions and were not moved during the taking of data. This was done by taking measurements

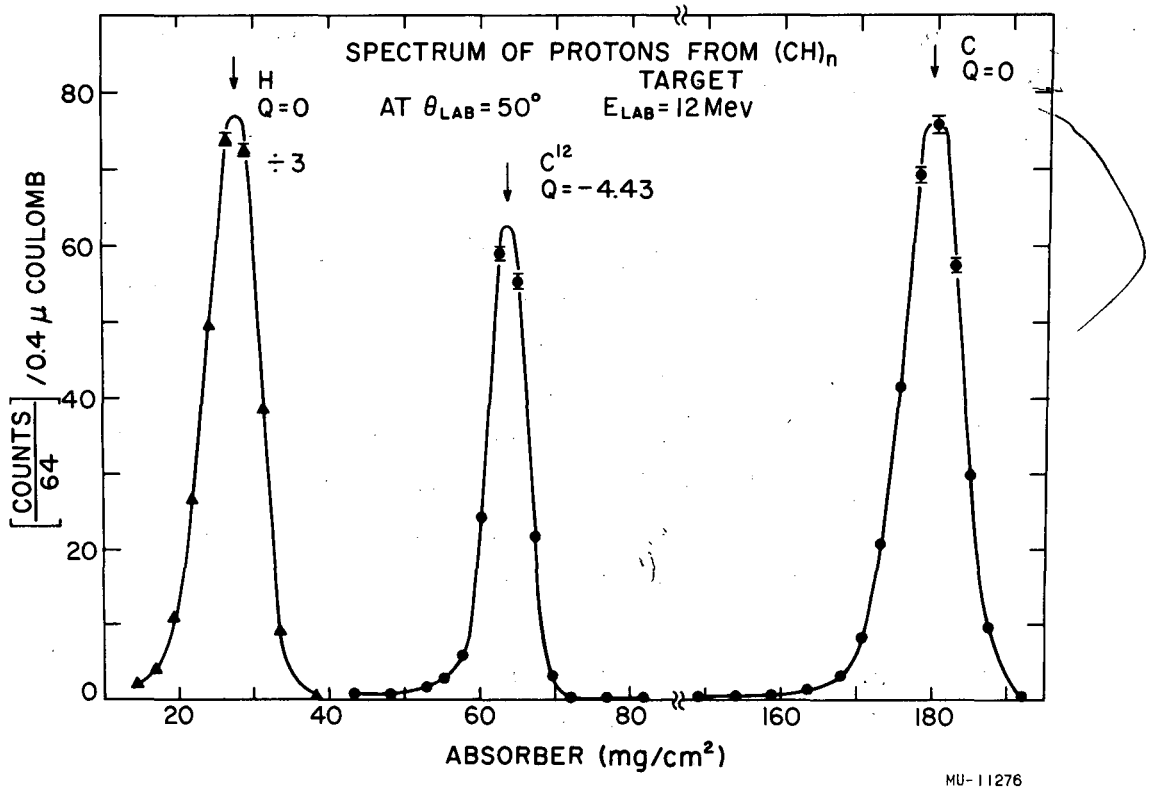

Fig. 5. Differential range spectrum of protons from CH target at $\theta_L = 50^\circ$.

from 7^{o} to 90^{o} on one side of the beam direction, and from 90^{o} to 167^{o} on the other side. In the lithium runs, measurements at angles forward of 45^{o} were made with the target perpendicular to the beam direction. On magnesium, this procedure was followed at angles forward of 30^{o}. In each case, data were taken at the same scattering angle both before and after the change in target angle was made. In this manner, the relative angular distribution for the forward angles could be normalized to that for the angles surveyed before the target was moved.

At regular intervals during the taking of data, especially when the counting rates were the highest, counts were taken with the gate pulse of counter No. 2 delayed several microseconds. The accidental coincidences obtained were always negligible.

III. REDUCTION OF DATA

A. Differential Cross Section

The differential cross section is given by the expression

$$\frac{d\sigma}{d\Omega} = \frac{N_s}{N\rho\Delta\Omega} ,$$

where N_s is the number of particles scattered into the solid angle $\Delta\Omega$,

N is the number of particles incident on the target,

ρ is the number of target nuclei per square centimeter,

$\Delta\Omega$ is the solid angle subtended by the detector collimator at the target.

In terms of measured and known quantities,

$$\rho = \frac{A_0 T F}{M \cos\theta_t} ,$$

where A_0 is Avogadro's number, T is the target thickness in g/cm^2, F is the fractional isotopic abundance of the particular target nuclei under investigation (e.g., 0.9248 for Li^7 in the lithium target), M is the molecular weight of the target material, and θ_t is the angle between the beam direction and the normal to the target surface. Also,

$$N_s = \frac{A}{\Delta R} \qquad \text{and} \qquad N = \frac{C\,V}{e} ,$$

where A is the area under the peak of the differential range curve, ΔR is the detector range bite, C is the beam-integrating capacitance in farads, V is the electrometer potential in volts, and e is the charge of the electron in coulombs. When these equations are combined, the differential cross section in the laboratory system is

$$\frac{d\sigma}{d\Omega} = \left(\frac{e\,M}{A_0\,T\,F\,\Delta R\,\Delta\Omega} \right) \frac{A \cos\theta_t}{C\,V} \quad \text{cm}^2/\text{steradian}.$$

The term in parentheses was constant for the run on each of the targets, and θ_t was changed only during the runs on lithium and magnesium, taking the values 0° and 45°.

Thus, to determine the differential cross sections the differential range curve of the appropriate proton group was taken at each angular setting of the detector. Smooth curves were drawn through the experimental points, and the areas under the curves were calculated by use of Simpson's one-third rule. Typical range curves of the proton groups measured are shown in Fig. 6. The calculated cross sections were then converted to the center-of-mass system, and these data comprise the final experimental results.

B. Errors

The expression for the differential cross section has the form of the product of several terms,

$$y = \prod_i x_i^{a_i} ,$$

for which the law of propagation of errors gives

$$\frac{\delta y}{y} = \left[\sum_i \left(a_i \frac{\delta x_i}{x_i} \right)^2 \right]^{1/2} .$$

In the following discussion the errors in the individual terms are considered separately.

The error in A, the area under a differential range peak, was from two contributing sources. One was the error in the estimate of the background subtraction. A smooth curve, usually a straight line, was drawn through the minima or the extended background level on both sides of the peak, thus defining the background level under the

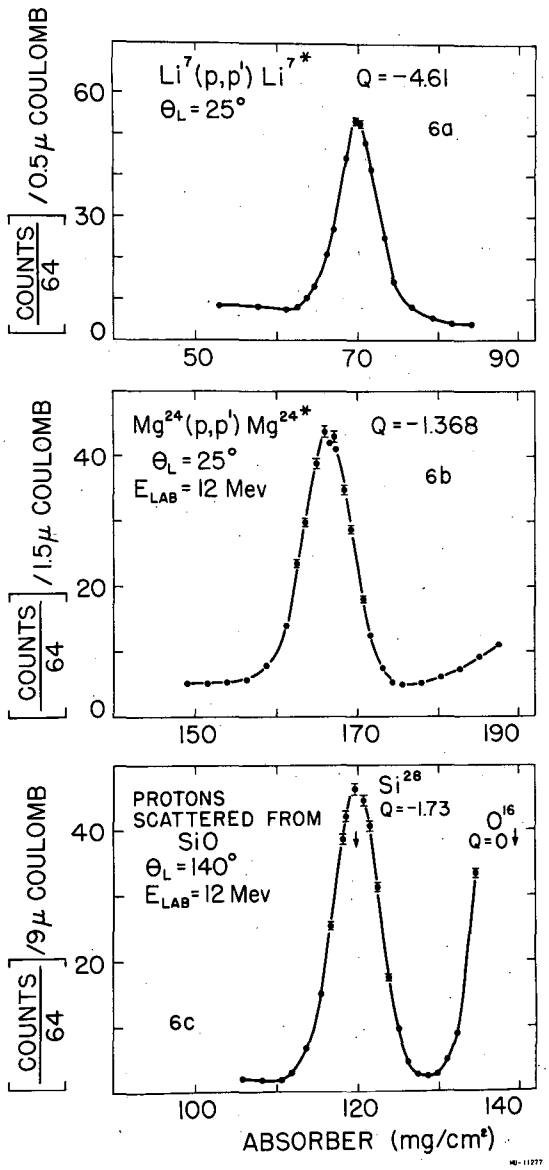

Fig. 6. Examples of the proton groups whose angular distributions were obtained.

peak. The possible error in the definition of this level was estimated, and the related error in A was calculated. The other source was the statistical counting errors on the points through which the peak itself was drawn. The relative error in the area, calculated by applying the law of propagation of errors to Simpson's formula, was related to the relative error in the peak point of the curve. This was done for several of the curves for each target. For each target, then, the determined relative error in area under a peak was plotted against the corresponding relative error in the peak point. Subsequently, smooth curves drawn through these plots were used to determine the relative error in area, corresponding to the known relative error in the peak point, for all the remaining range curves. Finally, the two contributing errors in the area were combined quadratically.

After several independent calibrations on C and V, the error in their product was estimated to be 0.5% in relative values and 0.75% in absolute values.

The maximum difference between indicated target angle and measured target angle was estimated to be 0.2°. This yields

$$\frac{\delta\ (\cos\ \theta_t)}{\cos\ \theta_t} = 0.35\%$$

for $\theta_t = 45^{\circ}$.

$\Delta\Omega$ was calculated from measurements of the diameter of the detector collimator aperture and its distance from the point where the beam passed through the target. The estimated uncertainty in these measurements gave

$$\frac{\delta\ (\Delta\Omega)}{\Delta\Omega} = 0.9\%.$$

The range bite ΔR was calculated from measurements of the area under a differential range curve and of the total number of particles in the corresponding group. Both these measurements included statistical counting errors. The combined errors gave

$$\frac{\delta\ (\Delta R)}{\Delta R} = 0.9\%$$

as a typical result.

With the exception of lithium, the target thickness, T, was determined from measurements of the area and the weight of a target section through which the beam had passed. The indirect method of measuring the lithium target thickness has been described previously. The results of estimated errors in the measurements were $\frac{\delta T}{T} = 5\%$ for lithium, 0.5% for carbon, 2.0% for magnesium, and 2.5% for silicon.

In making the transformation of the differential cross section from the laboratory system to the center-of-mass system, one multiplies by $f(\theta)$, a function of the laboratory scattering angle. Thus, the error in the determination of θ, $\delta\theta = 0.1^{\circ}$, yields the result

$$\frac{\delta f(\theta)}{f(\theta)} = 0.1\%.$$

IV. RESULTS AND CONCLUSIONS

A. General Considerations

Tables I through IV contain the experimentally determined differential and total cross sections for the inelastic scattering of 12-Mev protons to the 4.61-Mev level of Li^7, the 4.43-Mev level of C^{12}, the 1.368-Mev level of Mg^{24}, and the 1.78-Mev level of Si^{28}. Because the analysis of the results is concerned primarily with the shape of the angular distribution of the differential cross section, the errors in both the relative and absolute values of the cross sections were calculated. The relative errors alone are indicated on all plots of differential cross section versus center-of-mass scattering angle. This procedure serves to define more clearly the shape of the distribution.

At a laboratory angle of 30°, a differential range spectrum was taken which included the proton group corresponding to the excitation of the 7.65-Mev level of C^{12}. This spectrum is shown in Fig. 7. Hecht[12] had been unable to detect this group in the bombardment of carbon with 31-Mev protons. From the areas under the two

Table I

Differential cross sections for the reaction $Li^7(p,p')Li^{7*}$, Q = -4.61 Mev, in the center-of-mass system. E_{lab} = 11.95 ± 0.13 Mev.

θ_c (degrees)	$d\sigma/d\Omega$ (mb/sterad)	% errors $(d\sigma/d\Omega)$ relative	% errors $(d\sigma/d\Omega)$ absolute
9.3	9.18	3.8	6.4
11.8	9.45	3.4	6.2
17.7	9.93	2.2	5.6
29.6	10.07	1.9	5.4
41.2	9.73	2.8	5.9
52.7	9.28	2.0	5.5
64.0	8.84	1.6	5.4
75.0	7.97	1.5	5.4
85.6	7.38	1.7	5.5
93.4	6.78	1.4	5.3
101.1	6.50	1.5	5.4
110.9	6.54	1.4	5.3
120.4	6.43	1.3	5.3
129.5	6.43	2.8	5.9
138.4	6.16	2.2	5.6
147.0	5.84	1.3	5.3
155.4	5.44	3.8	6.5
163.7	5.23	5.9	7.8

Total cross section, σ_i = 95.1 ± 3.1 mb.

Table II

Differential cross sections for the reaction $C^{12}(p, p')C^{12*}$, $Q = -4.43$ Mev, in the center-of-mass system. $E_{lab} = 11.79 \pm 0.14$ Mev.

θ_c (degrees)	$d\sigma/d\Omega$ (mb/sterad)	% errors $(d\sigma/d\Omega)$ relative	$(d\sigma/d\Omega)$ absolute
7.7	40.2	5.7	5.9
11.0	41.3	4.5	4.7
13.1	40.7	2.7	3.1
16.3	39.3	3.3	3.7
21.9	38.5	2.8	3.2
27.4	35.2	2.8	3.1
32.8	32.7	2.0	2.5
38.1	28.90	1.4	2.0
49.0	22.53	1.1	1.8
54.3	20.46	2.0	2.5
64.9	16.01	1.9	2.4
75.3	12.64	1.4	2.1
85.6	10.60	1.3	1.9
95.6	9.82	1.4	2.0
105.6	11.08	1.8	2.3
115.3	14.84	1.7	2.0
124.9	18.97	1.7	2.2
134.3	23.47	1.2	1.9
143.7	28.10	1.1	1.9
152.9	30.8	1.3	2.0
162.0	33.3	1.9	2.4
166.5	32.9	2.4	2.8

Total cross section, $\sigma_i = 246.0 \pm 6.0$ mb.

Table III

Differential cross sections for the reaction $Mg^{24}(p, p')Mg^{24*}$; Q = -1.368 Mev, in the center-of-mass system. $E_{lab} = 11.87 \pm 0.08$ Mev.

θ_c (degrees)	$d\sigma/d\Omega$ (mb/sterad)	% errors $(d\sigma/d\Omega)$ relative	% errors $(d\sigma/d\Omega)$ absolute
15.5	39.9	5.1	5.6
20.7	28.7	4.4	5.0
31.0	16.15	2.8	3.7
41.3	12.54	2.3	3.3
49.3	12.15	2.3	3.3
56.6	12.00	2.6	3.5
63.7	13.61	2.4	3.4
67.8	15.76	2.5	3.5
71.8	22.51	2.3	3.3
81.9	25.39	2.2	3.3
92.0	23.59	2.2	3.3
102.0	17.49	1.7	3.0
111.9	14.10	3.1	4.0
121.7	14.59	2.1	3.2
131.5	18.72	2.2	3.3
141.3	21.65	1.5	2.9
151.0	19.65	1.9	3.1
157.8	17.15	3.3	4.1
165.5	13.14	6.1	6.5

Total cross section, $\sigma_i = 232.2 \pm 7.4$ mb.

Table IV

Differential cross sections for the reaction $Si^{28}(p, p')Si^{28*}$, Q = -1.78 Mev, in the center-of-mass system. $E_{lab} = 11.84 \pm 0.15$ Mev.

θ_c (degrees)	$d\sigma/d\Omega$ (mb/steradian)	% errors $(d\sigma/d\Omega)$relative	$(d\sigma/d\Omega)$absolute
15.4	24.44	6.2	6.8
20.5	23.74	3.7	4.7
30.9	22.67	1.9	3.5
41.2	21.10	2.3	3.7
51.6	18.34	2.2	3.6
61.8	15.91	1.8	3.4
72.0	12.64	2.0	3.5
82.2	10.95	1.8	3.4
92.3	9.43	2.1	3.6
102.2	7.85	2.5	3.8
112.1	7.00	2.9	4.1
117.0	6.96	2.9	4.1
125.7	7.27	2.2	3.6
131.6	7.64	2.0	3.5
141.3	11.04	1.8	3.4
150.9	14.61	2.1	3.6
160.6	18.31	3.7	4.7
167.3	18.19	4.6	5.4

Total cross section, $\sigma_i = 164.8 \pm 4.4$ mb.

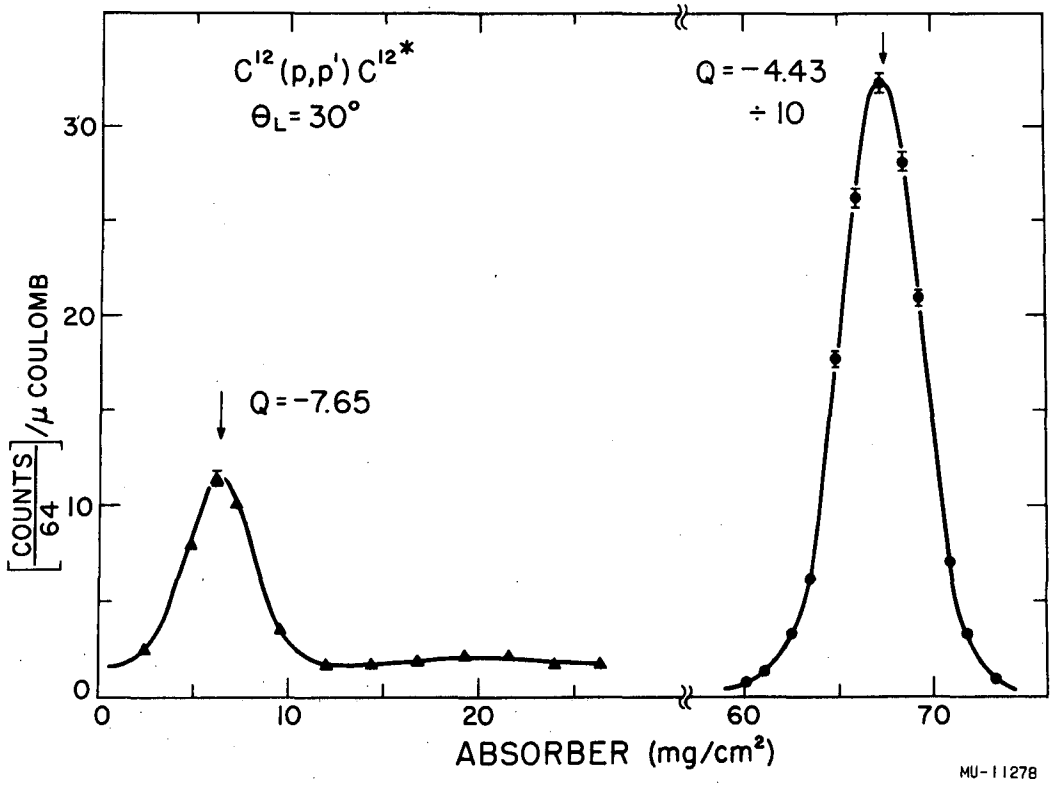

Fig. 7. Section of differential range spectrum of protons from CH target at $\theta_L = 30°$.

peaks in Fig. 7, one obtains directly the relative values of the differential cross sections for inelastic scattering to the two corresponding levels of carbon. Thus, at the laboratory angle of 30° the cross section for scattering to the 4.43-Mev level is 35 to 40 times as large as that for scattering to the 7.65-Mev level. No attempt was made to obtain the angular distribution of the smaller proton group because its mean range was below the range threshold of the detector at scattering angles exceeding 50°. Vaughn[17] has measured the angular distributions of 48-Mev alpha particles scattered inelastically from carbon, and his results are similar with respect to the ratio of the cross sections for the scattering to the two levels.

As was proposed in the introduction, the angular distributions have been analyzed in terms of the distributions given by the theory of the formation and decay of an intermediate (compound) nucleus and by the direct interaction theory of Austern, Butler, and McManus. This analysis, in terms of simple addition of the contributions from the two distinct mechanisms of inelastic scattering, is justified by the separate natures of the processes. In the direct interaction process the outgoing scattered part of the incident wave packet passes a given radius in a time $t \simeq \frac{h}{\Delta E}$, where ΔE is the spread in beam energy. The part of the incident pulse that forms a compound nucleus is not emitted before a time $t_c \simeq \frac{h}{D} \times \frac{1}{T}$, where $\frac{h}{D}$ is the "period of motion" in the compound state, D is the average level spacing, and T is the barrier transmission coefficient. The two outgoing pulses cannot interfere if $t_c > t$, or $\Delta E > DT$. This condition is satisfied in the cases covered by these experiments.

For each of the targets bombarded, the cross section for formation of the compound nucleus has been calculated by use of the asymptotic formula

$$\sigma_c \simeq \pi(a+\lambda\!\!\!^{-})^2 \left[1 - V/E \right],$$

where

$$a = 1.4 \times A^{1/3} \times 10^{-13} \text{ cm}, \quad V = Ze^2/(a+\lambda\!\!\!^{-}),$$

and E is the incident proton energy. This expression reproduces the more exactly calculated values within 15% for $E/V > 1.2$.[3] These

cross sections can be compared with the measured inelastic proton cross sections to give an estimate of the fraction of the reaction cross section contributed by this one decay mode. This expression for σ_c cannot be used, of course, where there is no overlapping of levels in the region of excitation of the compound nucleus.

B. Lithium

The angular distribution of protons corresponding to the excitation of the 4.61-Mev level of Li^7 is shown in Fig. 8. The excitation energy of the intermediate nucleus, Be^8, was 27.69 Mev, with an energy spread of about 120 kev in the proton beam. The statistical condition is assumed to be satisfied at this high excitation, yielding a contribution symmetric about $\theta = 90^\circ$ to the distribution. Because the experimental distribution shows a broad peak near the forward angles, $j_0^2(qa)$ proved to be the function that represented the contribution to the distribution from the direct interaction mechanism. In fitting the data, j_0^2 was calculated over a range of values of a, the nuclear radius. Each calculated j_0^2 was subtracted from the experimental distribution and the j_0^2 was selected that give a resulting curve (dashed in Fig. 8) symmetric about 90°. The best fit to the data was obtained with $a = 1.25\ A^{1/3} \times 10^{-13}$ cm, but values of a in the interval from $1.20\ A^{1/3} \times 10^{-13}$ cm to $1.35\ A^{1/3} \times 10^{-13}$ cm gave satisfactory agreement within the experimental errors assigned to the data.

The selection rules given by the direct-interaction theory can now be applied to give information about the 4.61-Mev level of Li^7. The rule governing the change of angular momentum (spin) between the initial and final states of the nucleus is

$$J_i + J_f + 1 \geq \ell \geq |\vec{J}_i + \vec{J}_f + \vec{l}|_{min},$$

and ℓ can take only odd or even values corresponding to a change or no change in parity between the states. Writing $|\vec{J}_i + \vec{J}_f| = \Delta J$ results in $\Delta J = \ell$ or $\ell \pm 1$. The value $\ell = 0$ has been determined from the order of the Bessel function that fits the data, therefore $\Delta J = 0, \pm 1$ with no parity change. The ground state of Li^7 is known to be a (3/2, -) state;[18] that is, its spin is 3/2 and its parity is odd. Thus, application of the selection rules above yields an assignment of J = 1/2, 3/2, or 5/2 and odd parity to the 4.61-Mev level of Li^7.

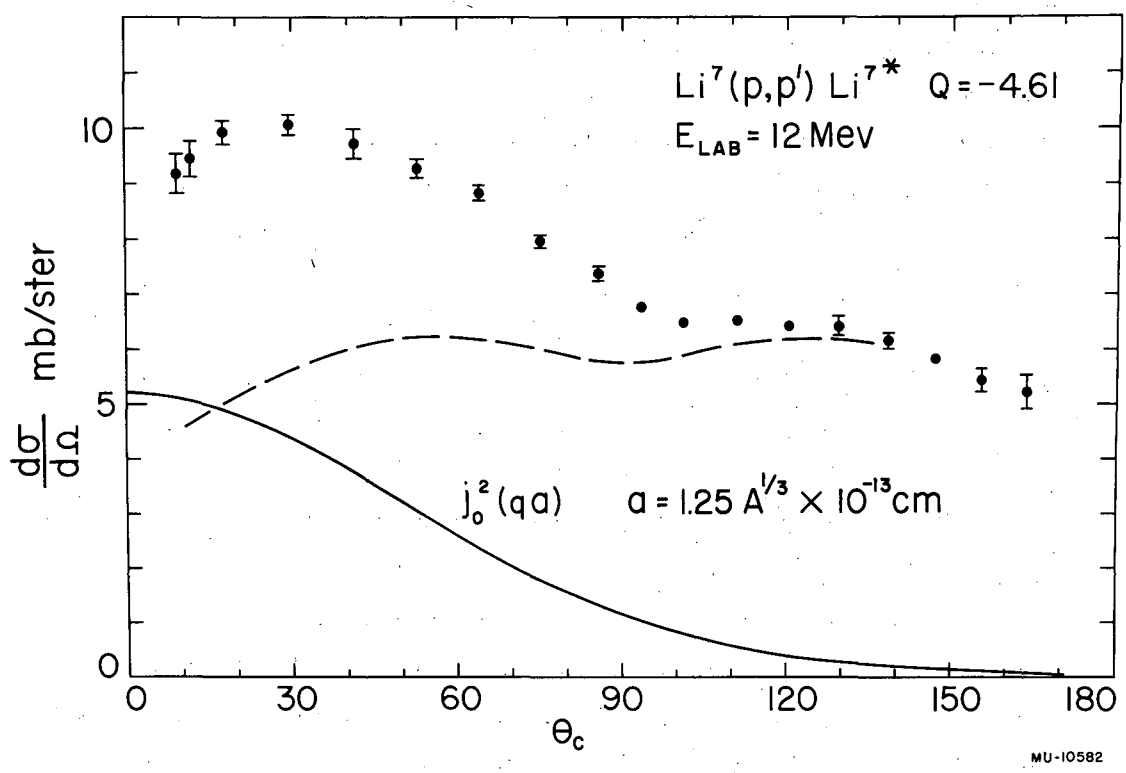

Fig. 8. Angular distribution of protons from the reaction $Li^7(p, p')\ Li^{7*}$, Q = -4.61 Mev.

Levine, Bender, and McGruer[19] have recently obtained an angular distribution of 14.5-Mev deuterons scattered from this level in Li^7. The differential cross section increases with center-of-mass angle in the interval from 17° to 90°, the extent of the distribution. The authors reported that the distribution was not in accord with the prediction of the theory of Huby and Newns,[20] which similarly describes inelastic deuteron scattering in terms of direct interactions at the nuclear surface.

The measured cross section for inelastic proton scattering to this level is $\sigma_i = 95.1 \pm 3.1$ mb, 80% of which is contributed by the component symmetric about $\theta = 90^\circ$. The result

$$\frac{\sigma_i(\text{sym})}{\sigma_c} = 0.16$$

indicates the strong competition provided by other modes of decay of the intermediate nucleus, the principal ones being neutron or proton emission leading to the formation of one of the several available states of Be^7 or Li^7.

C. Carbon

The angular distribution of protons corresponding to the excitation of the 4.43-Mev level of C^{12} is shown in Fig. 9. Fischer's data at 10 Mev[10] are plotted for comparison. Qualitatively, the shapes of the distributions are similar, each exhibiting peaks at forward and backward angles with the minimum near 95°. Also, the forward peak is the larger, thus the distribution is not symmetric about 90°. In addition to the increase in the cross section at 12 Mev, the forward peak has shifted approximately from 35° to 10° and the backward peak from 140° to 165° with the change in energy. At proton energies of 7.3 Mev,[8] 9.5 Mev,[11] and through the range from 14 Mev to 19.5 Mev[21] the distribution maintains the same general shape and indicates that the direct-interaction mechanism plays no important role. At 31 Mev[12] the distribution has changed markedly, becoming strongly peaked near the forward direction.

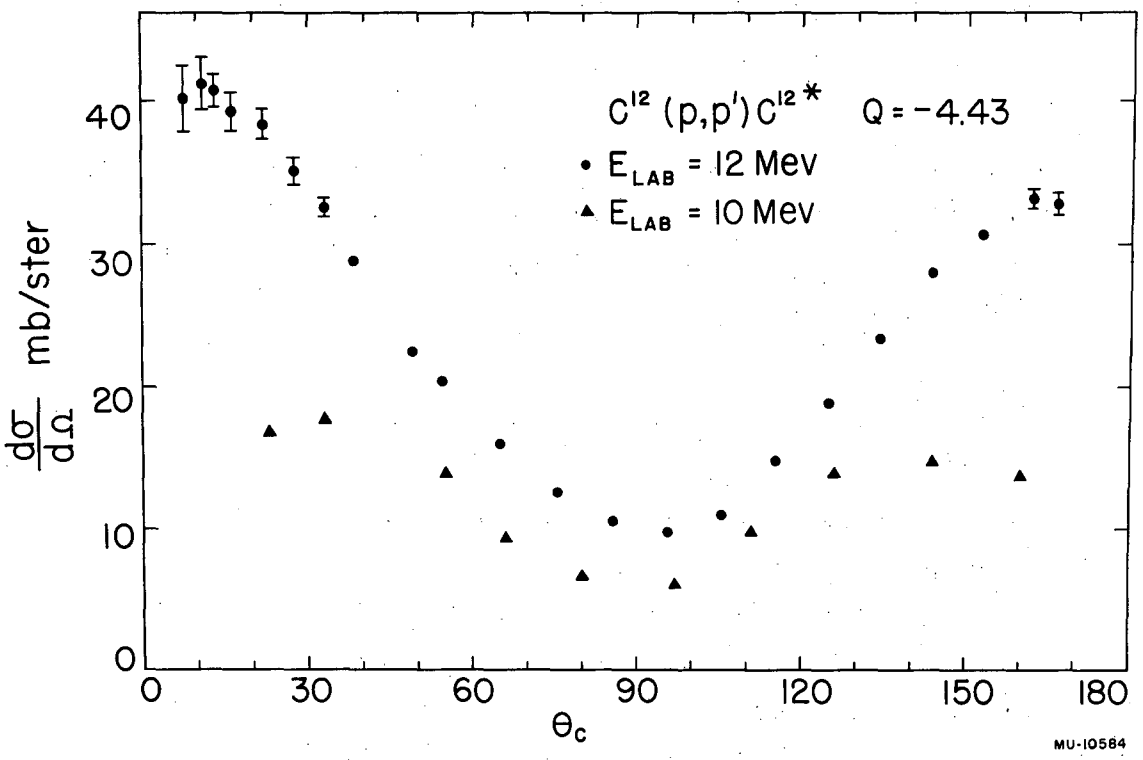

Fig. 9. Angular distribution of protons from the reaction $C^{12}(p, p')\, C^{12*}$, Q= -4.43 Mev.

The ground state of C^{12} is a (0, +) and the 4.43-Mev level is a (2, +) state.[18] Thus, $\Delta J = 2$ with no parity change; therefore, any contribution to the angular distribution from direct-interaction-type scattering would be given by $j_2^2(qa)$. This function is not peaked in the forward direction, and it proved to be impossible to fit the data of Fig. 9 with a j_2^2 in combination with a curve symmetric about 90°.

The excitation of the intermediate nucleus, N^{13}, was 12.82 Mev. There is little or no information available on the level structure of N^{13} at this excitation, but it can be inferred from the level scheme[18] of its mirror nucleus, C^{13}. It is apparent that no more than two or three levels take part in the reaction, so the statistical condition of many states' being excited is not satisfied. The situation probably is more nearly that one resonance in N^{13} is responsible for the major part of the cross section, with small additions coming from the wings of the neighboring resonances. This could explain both the near symmetry of the angular distribution and the fact that this near symmetry is maintained over such a large energy interval. The shifting of the peaks toward $\theta = 0^\circ$ and $\theta = 180^\circ$ with the increase in energy shows that the partial waves of higher orbital angular momentum are contributing more strongly to the reaction, as is possible at the higher energy.

The inelastic cross section measured was $\sigma_i = 246.0 \pm 6.0$ mb, and gave the results $\sigma_i/\sigma_c = 0.44$ and $\sigma_i(12 \text{ Mev})/\sigma_i(10 \text{ Mev}) \simeq 1.6$. The threshold for the (p, n) reaction is 18.5 Mev, so the only competing mode of decay of the compound nucleus was that of proton emission to the ground state of C^{12}, the so-called compound elastic scattering, which thus accounts for approximately 56% of the reaction cross section. We neglect the contributions of proton emission to the 7.65-Mev state (measured to be small) and to the 9.61-Mev state, the latter because of the small barrier transmission coefficients. A calculation was made to determine whether or not the large $\sigma_i(12)/\sigma_i(10)$ ratio could be explained in terms of barrier penetrability alone. Since $\sigma_c(10 \text{ Mev}) \simeq \sigma_c(12 \text{ Mev})$, one can make the approximation

$$\frac{\sigma_i(12)}{\sigma_i(10)} \simeq \frac{T_{(12)}}{T_{(10)}} ,$$

the ratio of the barrier transmission coefficients, at the two energies, for proton emission to the 4.43-Mev state. With the value $1.4 \times A^{1/3} \times 10^{-13}$ cm for the nuclear radius, these coefficients were calculated from tables of Coulomb functions.[22] The calculated ratio was

$$\frac{T_{(12)}}{T_{(10)}} = 1.5,$$

in fair agreement with the experimentally determined

$$\frac{\sigma_i(12)}{\sigma_i(10)}$$

. Also, it is quite reasonable that an increase in the inelastic cross section at 12 Mev could result from a more nearly resonant excitation of N^{13} at that energy.

D. Magnesium

The angular distribution of protons leading to the excitation of the 1.368-Mev level of Mg^{24} is shown in Fig. 10. The ground state of Mg^{24} is a (0, +) state and the 1.368-Mev level is a (2, +) state.[18] Thus, as for C^{12}, an appropriate fit to the data would be a combination of j_2^2 and a curve symmetric about 90°. The increase in the cross section forward of 40° ruled out this possibility.

Unlike the carbon distribution, the shape of the magnesium distribution apparently changes quite significantly with variation of the incident proton energy in the range from 4.7 to 12 Mev.[7-10] For example, at 10 Mev[10], peaks appear near 60° and 140° with a slight minimum at 105°. The differential cross section appears to be decreasing at 30°, but no data are plotted forward of that point. This variation is readily explained by assuming that several levels of the intermediate nucleus are excited, but not so many as to satisfy the statistical condition. Then the outgoing waves of different parity can interfere, giving asymmetric distributions. With the change in energy of the incident beam a different group of levels would be excited, the interference terms would have changed, and a completely dissimilar distribution could result. The formula

$$\omega(E) = 0.43 \exp[2(0.45\ E)^{1/2}]/\text{Mev}$$

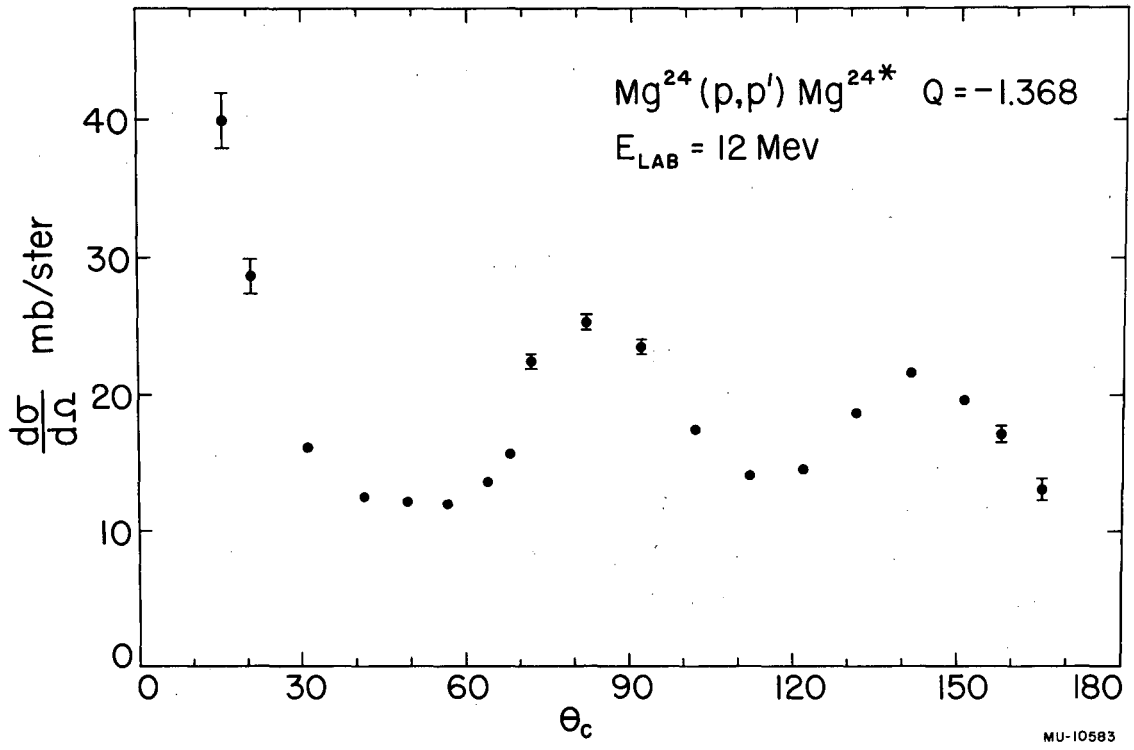

Fig. 10. Angular distribution of protons from the reaction $Mg^{24}(p, p')\,Mg^{24*}$, Q= -1.368 Mev.

agrees fairly well with the experimentally determined average level densities for Al^{27} at 9.0 Mev excitation, and therefore it is used to estimate the average level density for Al^{25} at 13.68 Mev, the excitation of our intermediate nucleus. The result is $\omega \simeq 60$ levels/Mev, so we estimate that approximately seven levels of the intermediate nucleus would be excited on the average. This hardly qualifies as "many" in the sense of the statistical assumption, and the region of excitation is certainly not the continuum where the level width exceeds the level spacing. Therefore, the statistical assumption probably should not be made.

The measured inelastic cross section was $\sigma_i = 232.2 \pm 7.4$ mb and $\sigma_i/\sigma_c \simeq 0.35$. The threshold for the (p, n) reaction is 14.6 Mev, so the competing processes are essentially only those of proton emission from Al^{25*} to the ground state and the several other available excited states of Mg^{24}. The smaller σ_i/σ_c compared with that for carbon indicates the larger number of proton emission possibilities. The ratio

$$\frac{\sigma_i(12 \text{ Mev})}{\sigma_i(10 \text{ Mev})} \simeq 1.1$$

was calculated by integrating over the range of angles covered by the 10-Mev data, thus the forward peak at 12 Mev was not included. This value is readily explained as a consequence of the slightly larger barrier transmission coefficient at the higher energy.

E. Silicon

The angular distribution of protons corresponding to the excitation of the 1.78-Mev level of Si^{28} is shown in Fig. 11. A satisfactory fit to the data was made with the combination of a contribution symmetric about 90° and a $j_1^2(qa)$ for a value of $a = 1.25\ A^{1/3} \times 10^{-13}$ cm. The analysis was very sensitive to variations in a because slight shifts in the position of the j_1^2 peak destroyed the symmetry of the dashed curve. For example, values of $a = 1.20\ A^{1/3} \times 10^{-13}$ cm and $1.30\ A^{1/3} \times 10^{-13}$ cm gave appreciably poorer results in fitting the data.

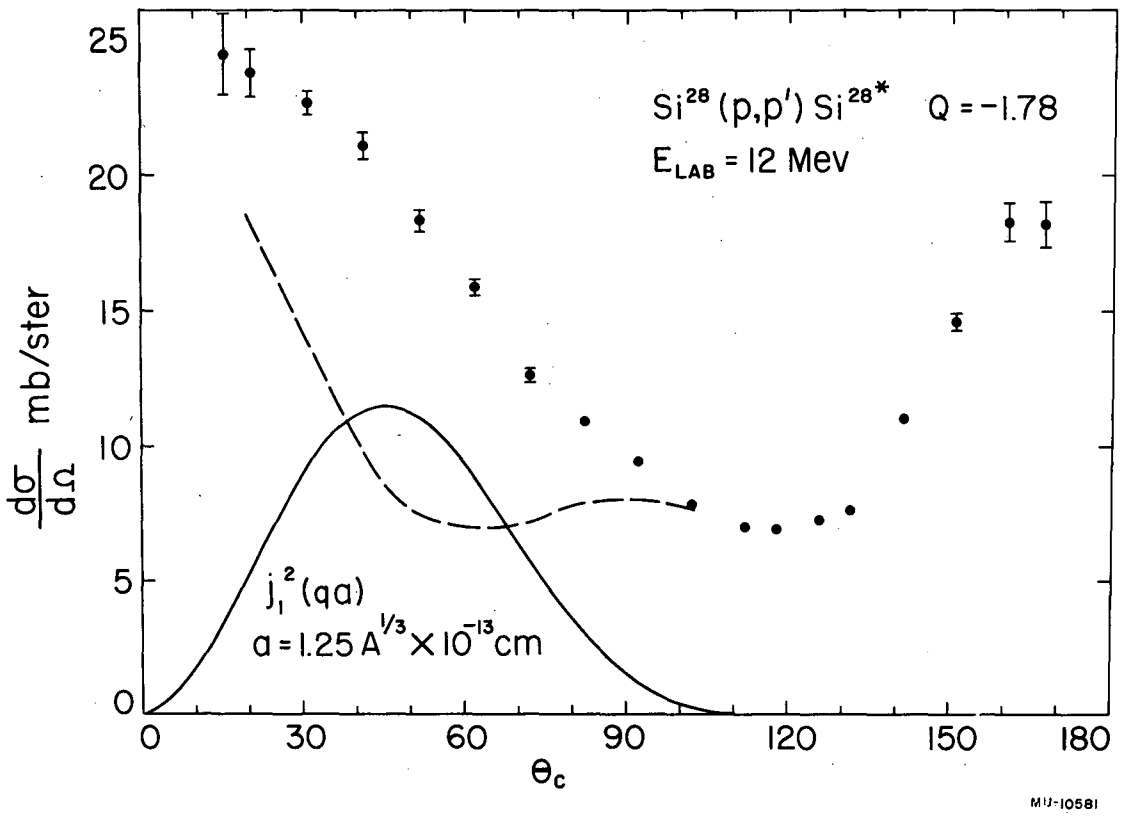

Fig. 11. Angular distribution of protons from the reaction $Si^{28}(p, p')\,Si^{28*}$, Q= -1.78 Mev.

The ground state of Si^{38} is a(0, +) state and the 1.78-Mev level is a(2, +) state.[18] Thus, $\Delta J = 2$ with no parity change between the two states. As before, the selection rules require the order of the Bessel function (describing the direct-interaction distribution) to be $\ell = 2$. It was not possible to fit the data with a j_2^2 function because its peak is too narrow when a is chosen so that the peak falls near 45° as is required. The value $\ell = 1$ satisfies the selection rule on angular momentum, $\Delta J = \ell$, $\ell \pm 1$ but this odd value of ℓ is ruled out by the selection rule on parity.

At the 14.14-Mev excitation of the intermediate nucleus, P^{29}, it is estimated that approximately 10 levels would be excited. In view of the asymmetry of the magnesium angular distribution, it would be too much to expect that the statistical condition be met by the excitation of several more levels in the case of inelastic scattering on silicon. However, the fact that the silicon distribution is somewhat closer to symmetry about 90° suggests an approach toward that condition.

The integrated inelastic cross section was $\sigma_i = 164.8 \pm 4.4$ mb and $\sigma_i/\sigma_c \simeq 0.25$. Since the threshold for the (p, n) reaction is 14.9 Mev, there is again no neutron emission from the P^{25*} nucleus competing with the proton emission to the ground state and the available excited states of Si^{28}.

F. Conclusions

The observed angular distribution of protons scattered inelastically from Li^7, leading to the formation of the 4.61-Mev state, is in agreement with the prediction based on the statistical theory of the compound nucleus and of the Austern, Butler, and McManus theory. Distributions of protons scattering to levels in C^{12}, Mg^{24}, and Si^{28} are not explained by either or both of the theories. It is thought that the statistical theory is not applicable because the required condition that the reaction proceed via the continuum region of the intermediate nucleus is not fulfilled. Since C^{12}, Mg^{24}, and Si^{28} are tightly bound even-even nuclei, it follows that the direct-interaction mechanism could be almost completely suppressed and the incident proton be captured by the target nucleus whenever it reached the nuclear surface.

It is suggested that the reactions involving these nuclei proceed by way of only a few levels of the intermediate nucleus.

It is reasonable that the direct-interaction type of theory could be applied more successfully to the inelastic scattering of deuterons and alpha particles. Competition from formation and subsequent decay of an intermediate nucleus would be slight, because once a deuteron or alpha particle had been captured by the target nucleus there would be little probability of its reemission. The experimental results of inelastic alpha-particle scattering from carbon and magnesium,[17] inelastic deuteron scattering from carbon,[23] and inelastic alpha-particle and deuteron scattering from beryllium[24] confirm this belief.

ACKNOWLEDGMENTS

It is a distinct pleasure to thank Professor A. C. Helmholz for his guidance, encouragement, and consistent interest in all phases of the work; Dr. Robert E. Ellis, Dr. Frank J. Vaughn, and Mr. Robert G. Summers-Gill for their active participation in obtaining the data; the late G. Bernard Rossi, Mr. William B. Jones, and the members of the 60-inch cyclotron crew for their continuous and most successful efforts in providing optimum cyclotron operation; Mr. Daniel J. O'Connell for preparing the SiO target; and Mr. Fred E. Vogelsberg for his maintenance of the electronic equipment.

This work was done under the auspices of the U. S. Atomic Energy Commission.

References

1. T. R. Wilkins and G. Kuerti, Phys. Rev. 57, 1082 (1940). C. F. Powell et al., Nature 145, 893 (1940).
2. N. Bohr, Nature 137, 344 (1936).
3. J. M. Blatt and V. F. Weisskopf, "Theoretical Nuclear Physics," New York, Wiley, 1952.
4. L. Wolfenstein, Phys. Rev. 82, 690 (1951).
5. N. Austern, S. T. Butler, and H. McManus, Phys. Rev. 92, 350 (1953).
6. M. G. Mayer, Phys. Rev. 75, 1969 (1949). O. Haxel, J. H. D. Jensen, and H. E. Suess, Phys. Rev. 75, 1766, (1949).
7. E. H. Rhoderick, Proc. Roy. Soc. (London) 201, 348 (1950).
8. H. E. Gove and H. F. Stoddart, Phys. Rev. 86, 572 (1952).
9. C. J. Baker, J. N. Dodd, and D. H. Simmons, Phys. Rev. 85, 1051 (1952).
10. G. E. Fischer, Phys. Rev. 96, 704 (1954).
11. W. Burcham, W. M. Gibson, and J. Rotblat, Phys. Rev. 92, 1266 (1953).
12. G. J. Hecht, Angular Distributions of Charged Particles from 31-Mev Protons on Carbon (Thesis), UCRL-2969, April 1955.
13. G. Schrank, P. C. Gugelot, and I. E. Dayton, Phys. Rev. 96, 1156 (1954).
14. R. G. Finke, Charged Particles from Beryllium Bombarded by 31.3 -Mev Protons (Thesis), UCRL-2789, Nov. 1954.
15. R. E. Ellis, Elastic Scattering of 48-Mev Alpha Particles by Heavy Nuclei (Thesis), UCRL-3114, Aug. 1955.
16. W. A. Aron, B. G. Hoffman, F. C. Williams, AECU-663 (1949).
17. F. J. Vaughn, Elastic and Inelastic Scattering of 48-Mev Alpha Particles by Carbon and Magnesium (Thesis), UCRL-3174, Oct. 1955.
18. F. Ajzenberg and T. Lauritsen, Revs. Modern Phys. 27, 77 (1955).
19. S. H. Levine, R. S. Bender, and J. N. McGruer, Phys. Rev. 97, 1249 (1955).

20. R. Huby and C. H. Newns, Phil. Mag. 42, 1442 (1951).
21. Conference, Brookhaven National Laboratory (January 1955) on "Statistical Aspects of the Nucleus," p. 86.
22. I. Bloch, et al., Revs. Modern Phys. 23, 147 (1951).
23. R. G. Freemantle, W. M. Gibson, and J. Rotblat, Phil. Mag. 45, 1200 (1954).
24. R. G. Summers-Gill (to be published).